Journal of Renewable Materials

Tech Science Press

DOI: 10.32604/jrm.2023.027592

ARTICLE

Effect of CSH Crystal Nucleus on Steam-Free Cured Fly Ash Precast Concrete Components

Ruyi Luo, Yanyan Hu*, Tingshu He*, Xiaodong Ma and Yongdong Xu

College of Materials Science and Engineering, Xi'an University of Architecture & Technology, Xi'an, 710055, China

*Corresponding Authors: Yanyan Hu. Email: huyy@sina.com; Tingshu He. Email: hetingshu@xauat.edu.cn

Received: 05 November 2022 Accepted: 05 December 2022 Published: 20 July 2023

ABSTRACT

The measures of steam curing and early-strengthening agents to promote the precast components to reach the target strength quickly can bring different degrees of damage to the concrete. Based on this, the new nanomaterial CSH-the hydration product of cement effectively solves these measures' disadvantages, such as excessive energy consumption, thermal stress damage, and the introduction of external ions. In this paper, the effect of CSH on the early strength of precast fly ash concrete components was investigated in terms of setting time, workability, and mechanical properties and analyzed at the microscopic level using hydration temperature, XRD, and SEM. The results showed that under the same workability, CSH could significantly reduce the amount of admixture, shorten the final setting time, almost not affect the initial setting time, and accelerate the hydration of cement. At the optimum dose of 5%, the mechanical properties of the specimens were improved by more than 98% within 12 h of hydration, resulting in an earlier release time of 12 h and no risk of strength inversion later. The results of this paper give theoretical support to the behavior of precast components under steam-free curing.

KEYWORDS

Fly ash concrete; prefabricated components; steam-free curing; CSH crystal nucleus; tobermorite

1 Introduction

The demand for concrete in the modern construction industry has increased dramatically [1], and the consumption of Portland cement, as the primary cementing material of traditional concrete, has also increased dramatically. However, the production of Portland cement consumed many non-renewable resources, such as coal and limestone, but also negatively impacted the environment. It was reported that 90% of industrial CO_2 emissions were generated during the production of Portland cement [2], accounting for 5%–8% of the world's total CO_2 emissions and 5%–6% of the total SO_2 emissions [3,4]. If industrial by-products (such as slag, fly ash and silica fume) were used as supplementary cementing materials to replace part of Portland cement, greenhouse gas emissions and energy consumption could be significantly reduced [5–7]. Compared with other supplementary cementing materials, fly ash had the advantage of low prices and ample storage [8,9], and fly ash could improve concrete workability and durability [10–14]. However, due to the low pozzolanic activity of fly ash, the early mechanical properties of concrete were poor [15–17], which would considerably delay the time when the concrete reached the target strength, thus affecting the construction progress and the turnover of formwork.

High-temperature steam curing was an effective way to improve the early strength of concrete [18,19]. However, steam curing would consume a lot of energy, cause environmental impact and increase economic costs. Steam curing also brought some defects to concrete, such as thermal damage, brittle increase and strength shrinkage of concrete [20,21]. Another way was to add early strength agents to the concrete [22–25], which could shorten the demolding time of prefabricated components steam-free curing. However, traditional inorganic salt early strength agents such as chlorine salts would increase the Cl^- permeability coefficient of concrete and seriously affect the durability of reinforced concrete [26,27]; Sulfates were prone to microcracks and strength reversion [28]; The use of organic alcohol amine early strength agents was complex and sensitive to the dosage, which was difficult to control in practical application, and was easy to cause retarding or even rapid setting [24,29]. Therefore, finding a new way to improve the early strength of concrete steam-free curing was necessary.

The rapid development of nanomaterials has brought technological innovation to the traditional concrete industry [30]. Some nanomaterials have been introduced into concrete for research, such as nano-SiO_2, nano-Al_2O_3, nano-TiO_2, and nano-$CaCO_3$ [31,32]. The application of nanomaterials in concrete means that the matrix could be modified at the nanoscale, which could significantly improve the performance of cement-based materials [33,34]. For example, nano-SiO_2 could react with calcium hydroxide in concrete, which could significantly improve the performance of the interface transition zone. Nano-CSH has recently been considered one of the most promising admixtures [35–37]. Several studies [38–42] reported the effect of nano-CSH on the hydration reaction of cement. Added CSH to cement paste to accelerate the hydration reaction of cement minerals, reduce the volume fraction of harmful pores and increase the early compressive strength. Li et al. [38] prepared nano-CSH seed by separate nucleation and growth phase separation using tartaric acid as a stabilizer and found that the addition of CSH seed promoted the hydration reaction of cement paste and reduced the maximum peak of heat flow and the time required to reach the maximum peak. They also reduced the volume fraction of large capillaries, and increased the volume fraction of medium capillaries and small mesopores, increasing the compressive strength of the hardened cement stone at all ages. Gu et al. [39] used ground granulated blast furnace slag and calcium carbide slag as raw materials and ground them in a ball mill along with a certain amount of water and polycarboxylic acid water-reducing agent to obtain CSH particles with a particle size of 420 nm. The effect of CSH on the mechanical properties of the mortar was further investigated. It was found that 2%–4% CSH increased the 1 d strength by 28.8%–37.1%, reduced the volume fraction of harmful pores from 45% to 29%–4%, and increased the volume fraction of harmless pores from 49.8% to 89.2%–89.9%.

Unlike the CSH seed prepared by Li et al. [38] and Gu et al. [39] in an amorphous or semi-crystalline state, Wang et al. [40] prepared highly crystalline CSH nanoparticles by hydrothermal synthesis at 120°C. CSH particles significantly accelerated the hydration of C3S by the heat of the hydration test, 3% of CSH particles increased the exothermic rate from 2.62 to 3.54 mW/g, and the 1 d compressive strength increased by 43%. On the other hand, Wang et al. [41] reported the effect of C-S-H-PCE nanocomposites on the early mechanical properties of mortars with different water-cement ratios and found that the enhancement effect of C-S-H-PCE was more evident at lower water-cement ratios. C-S-H-PCE also reduced the total porosity and decreased the average pore size, which had a more pronounced effect as the water-cement ratio was reduced. In addition, studies have also reported the effect of CSH seed on cementitious properties in the presence of mineral admixtures [42]. The results showed that 4% CSH seed increased the compressive strength of cement paste containing 20% fly ash by 329% and 172% at 8 and 12 h, respectively, and the tensile strength by 125% and 57%, respectively, and reduced the 90 d rheological shrinkage value of the samples by about 10%. This shows that the nano-CSH seed is effective in hydrating pure cement and performs well in the presence of mineral admixtures. Moreover, the study by Wang et al. [43] showed that the newly formed C-S-H gels were directly precipitated on the surface of

the added CSH seed, which provided conclusive evidence for the nano-CSH particles as liquid phase nucleation seed.

The studies mentioned above showed that the presence of nano-CSH seed brings a positive impact on cement hydration as well as pore structure. The nano-CSH has a similar structure and components to the cement hydration product C-S-H gels [35] with an autocatalytic acceleration process. At the same time, the nano-CSH particles could act as nucleation seed in the liquid phase, providing nucleation sites for the hydration products and thus accelerating the cement hydration process. Therefore, the direct use of nano-CSH could give better results than other early promoter [44] and does not have adverse effects due to introducing other harmful ions. In the past, more attention has been paid to the synthesis of nano-CSH and its role in the cementitious base. However, the effect of nano-CSH on highly doped mineral admixture concrete has rarely been reported, especially in applying highly doped fly ash precast concrete.

This paper aimed at the problem that the mechanical properties of fly ash concrete prefabricated components were insufficient at the early age under the condition of steam-free curing, a new nanomaterial-CSH introduced to study its role in cement further and reveal its influence on cement hydration process and microstructure. This may help replace the traditional industrial technology, promote the development of the early strength of the prefabricated components, enable the prefabricated components to demold as soon as possible under the condition of steam-free curing, improve the use efficiency of the formwork, and save energy consumption at the same time. It provided more theoretical guidance for preparing steam-free curing prefabricated components.

2 Materials and Methods

2.1 Materials

The raw materials used in this study were Ordinary Portland cement and Class II fly ash provided by Jidong Cement Co., Ltd. (Datong, China). The chemical compositions and particle size distribution of cement and fly ash are listed in Table 1 and Fig. 1, respectively. The additives VIVID-651 polycarboxylic acid superplasticizer and VIVID-300 crystal nucleus (CSH) used in the study were provided by Shanghai Sanrui Polymer Materials Co., Ltd. (China). The solid content of the VIVID-651 polycarboxylic acid superplasticizer was 10%, and the water reduction rate was 30%. VIVID-300 nuclei are stable suspensions of CSH nanoparticles in a semi-crystalline state, with Ca/Si of 1.5 and solid content of 20%, miscible with water. The sand was river sand with a fineness modulus of 2.8, and the coarse aggregate was gravel with a continuous particle size distribution of 5–20 mm.

Table 1: Chemical compositions of cement and fly ash

Chemical compositions		CaO	SiO_2	Al_2O_3	Fe_2O_3	MgO	SO_3	Na_2O	K_2O	TiO_2
Cement	Content (wt%)	63.56	19.17	4.75	4.32	2.22	3.38	0.43	1.28	0.36
Fly ash		4.45	54.46	21.70	8.85	1.48	1.59	1.03	3.85	1.60

2.2 Methods

2.2.1 Mix Proportion

The concrete sample mix used for the compressive strength test and workability analysis is shown in Table 2. VIVID-300 crystal nucleus content is 0%–7% of the total mass of the gelling material. VIVID-651 superplasticizer was used to make each group of fresh concrete have a similar slump. The test samples used for setting time, hydration temperature, FTIR, XRD, and SEM were the paste samples with the same proportion.

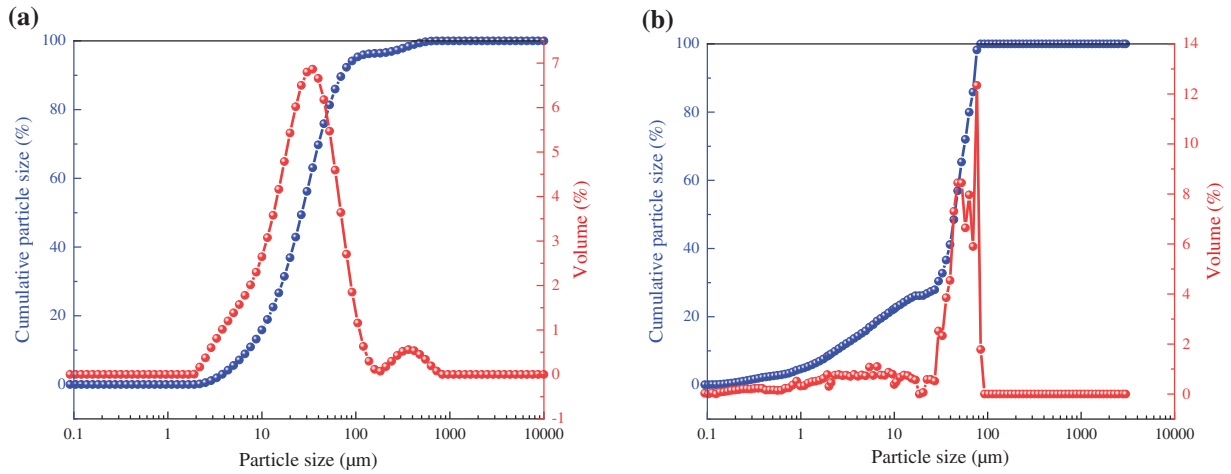

Figure 1: Particle size distribution of cement (a) and fly ash (b)

2.2.2 Workability

By adjusting the dosage of VIVID-651 superplasticizer, the concrete slump of each group was kept at 150 ± 10 mm. Through this, we could get the changing trend of the superplasticizer amount and reflect CSH's influence on the workability of fresh concrete.

2.2.3 Setting Time

There was a certain correlation between the speed of paste setting and the development of the early strength of concrete. According to Chinese National Standard GB/T 1346-2011, the setting time of the paste was measured by the Vicat apparatus. When the initial setting needle was 4 ± 1 mm away from the base plate, it was considered that the sample had an initial setting. And then, the final setting time was measured. There was no ring mark on the surface. The final setting time was reached.

2.2.4 Hydration Temperature

Mixed the powder to be measured evenly and then put into a cylindrical container with a size of Φ 85 × 85 mm after adding water and stirring. The container was then placed in a thermostat at a temperature of 20°C ± 0.5°C, placed a thermocouple in the center of the paste to transmit the real-time change of the center temperature during hydration to the recorder. The test time was 36 h, and the temperature collection interval was 20 s. The test setup is shown in Fig. 2.

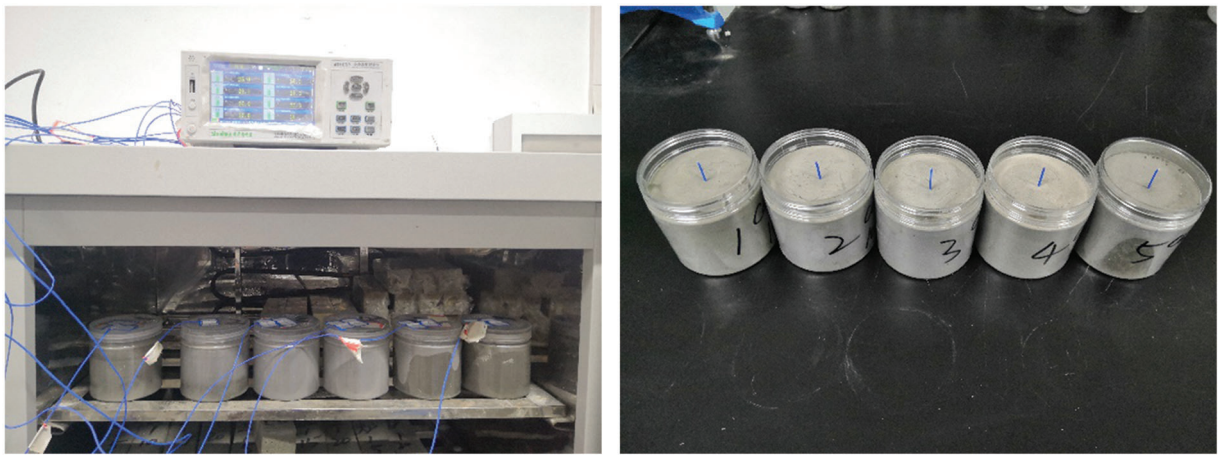

Figure 2: Hydration temperature testing device and test samples

2.2.5 Compressive Strength

Refer to Chinese National Standard GB/T 50081-2019 to make specimens with a size of 100 mm × 100 mm × 100 mm to test the compressive strength of concrete. After the samples were made, they were covered with cling film to prevent the evaporation of moisture from the surface of the specimens. They were then placed in the forming chamber for natural curing (natural temperature of 20°C ± 2°C and humidity of 50% ± 2%) until 8, 12 and 24 h, when they were tested for compressive strength. The rest of the specimens were demoulded after 24 h and then transferred to a standard curing chamber at a temperature of 20°C ± 2°C and a humidity of 95% or more until 3, 7 and 28 d, respectively, when they were tested for compressive strength.

2.2.6 Micro Test

The instrument model used for the Fourier transform infrared spectroscopy (FTIR) test was Bruker Vertex 70, and the test range was 400–4000 cm^{-1}. The equipment model of XRD detection was the Brooke D8. The setting angle was 2, the scanning range was 5°–60°, and the step size was 0.02°/step. The ZEISS Gemini 300 SEM-EDS scanning electron microscope was used to analyze the hydration products' microscopic morphology and energy spectrum.

3 Results and Discussion

3.1 Workability

The concrete slump of the reference concrete was 150 ± 10 mm, so the concrete slump containing CSH was consistent with that of the reference concrete. In Table 2, with the increase of CSH content, the amount of superplasticizer decreased. Compared with the reference concrete, the concrete with 1%, 3%, 5%, and 7% CSH could reduce the superplasticizer dosage by 20%, 27%, 40%, and 47%, respectively. CSH could improve the concrete operating performance and reduce the superplasticizer amount to ensure that the slump was unchanged. Because superplasticizers were used as dispersants for preparing CSH [45,46], this dispersant could disperse the nanoparticles. Some dispersants were adsorbed on the surface of cement particles, which could disperse and act as a water reducer.

Table 2: Mix proportion of single concrete (kg/m^3)

Mix ID	Cement	Fly ash	Sand	Gravel	Water	VIVID-300	VIVID-651	W/B
CSH0	293	158	762	1052	162	0	7.49	0.36
CSH1	293	158	762	1052	162	1%	6.00	
CSH3	293	158	762	1052	162	3%	5.48	
CSH5	293	158	762	1052	162	5%	4.51	
CSH7	293	158	762	1052	162	7%	4.01	

3.2 Setting Time

Fig. 3 shows the setting time change of cement paste with different CSH contents. Overall, with the increase in the content of CSH, the system's initial setting time and final setting time showed a shortening trend. For cement paste without CSH, the initial setting time was 242 min, and the final setting time was 313 min. When 1%, 3%, 5%, and 7% of CSH were added, the initial setting time was reduced by 1.2%, 1%, 6.7%, and 7.5%, respectively; and the final setting time was reduced by 2.5%, 6.5%, 10%, and 16.5%, respectively. CSH had a noticeable accelerating effect on the paste, especially in shortening the final setting time. Because CSH accelerated the hydration reaction of the paste [47], the rapid formation of C-S-H gel connected cement and fly ash particles, thus shortening the setting time of the paste. Other Scholars have also reached similar conclusions [36,41].

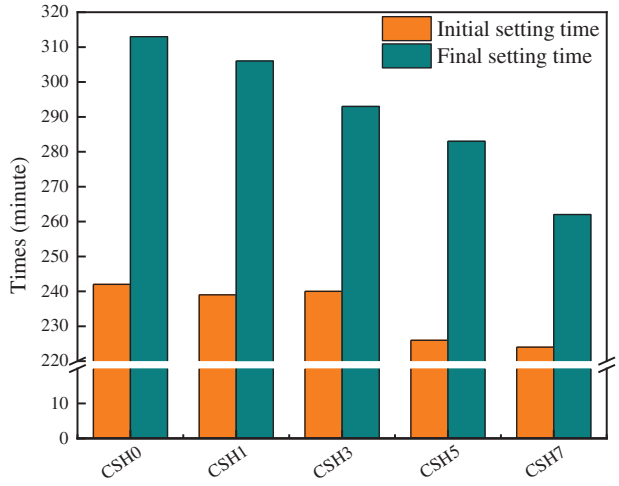

Figure 3: Effects of CSH on the setting time of cement paste

3.3 Compressive Strength

The strength development of concrete modified with CSH was shown in Fig. 4. The average compressive strengths of the concrete without CSH were 2.5, 8.0, 18.6, 26.2, 40.5, and 48 MPa at 8 h, 12 h, 24 h, 3 h, 7 h, and 28 d, respectively. When 1%, 3%, 5%, and 7% of CSH were added, the compressive strengths were increased by 22%, 184%, 196%, and 252% at 8 h, respectively, and by 15%, 25%, 98%, and 104% at 12 h, respectively. The strength of concrete with 5% and 7% of CSH at 12 h age met the release strength (≥15 MPa) required by Chinese National Standard GB/T 51231-2016. CSH could significantly reduce precast concrete demolding time and increase formwork turnover efficiency. From Fig. 4b, it can be seen that CSH enhanced the early strength while ensuring that the 28 d strength does not decrease. Specifically, CSH added at 1%, 3%, 5%, and 7% still showed positive growth in compressive strength at 28 d, increasing by 3%, 5%, 7%, and 4%, respectively, compared with the reference concrete.

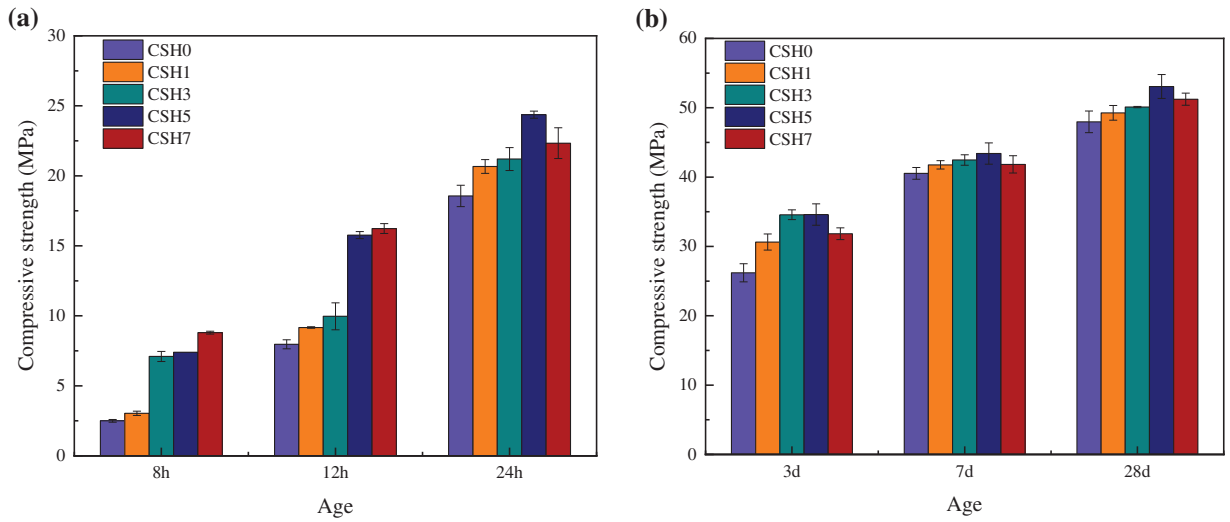

Figure 4: Effects of CSH on the strength of concrete: (a) curing for 8, 12, 24 h, (b) curing for 3, 7, 28 d

The presence of CSH stimulated the hydration reaction of cement, provided more nucleation sites for hydration products [48,49], and reduced the potential nucleation barrier of hydration products [48,50]. C-S-H gel nucleated and grew on the surface of cement minerals but also grew more easily on the surface of CSH particles [51], which significantly accelerated the early hydration of cement. Concrete generated a large amount of C-S-H gel in a relatively short time, and adjacent sites were interwoven into a three-dimensional structure through C-S-H gel, which also promoted the polymerization of silicon-oxygen bonds in C-S-H gel and further generated more high-quality C-S-H so that concrete could obtain higher compressive strength. It is worth mentioning that the best content of CSH was 5% of the cement mass. Because it can significantly reduce the demolding time of the precast concrete parts and, at the same time, has the most apparent effect on the later strength improvement.

3.4 Hydration Temperature

The hydration temperature reflected the heat release of the hydration reaction in the system, and the hydration rate of cement was completely consistent with the heat release of hydration. Therefore, the hydration temperature also indirectly reflected the hydration rate of cement paste. From Fig. 5, the addition of CSH crystal seed significantly increases the height of the main peak, and the slope of the heat flow curve shortens the induction period and brings forward the appearance of the exothermic peak. The exothermic hydration peak of the control group reached the maximum value in 19.1 h, at which time the maximum temperature was 25.8°C, and the overall exothermic peak showed a gentle rise and fall. When 1%, 3%, 5%, and 7% of CSH were added, the appearance time of the exothermic hydration peak was 17.5, 16.2, 14.5, and 13.5 h, which was shortened by 8.4%, 15.2%, 24.1%, and 29.4%, respectively, compared with the reference concrete. The results showed that the CSH crystal seed obviously accelerated the hydration of C_3S and promoted the formation of new C-S-H. This effect was more obvious when a higher content of CSH crystal seed was added. From the results of Wang et al. [43], the CSH crystal seed act as a nucleation center and dispersing agent in cement paste. Since the presence of nucleation and growth sites—CSH crystal seed, the formation of hydration products moved away from the surface of the clinker, resulting in the dissolving barrier being lowered [47]. Therefore, when CSH crystal seeds are present, the hydration process is accelerated, including the increase of peak hydration exothermic heat and the decrease of the induction period.

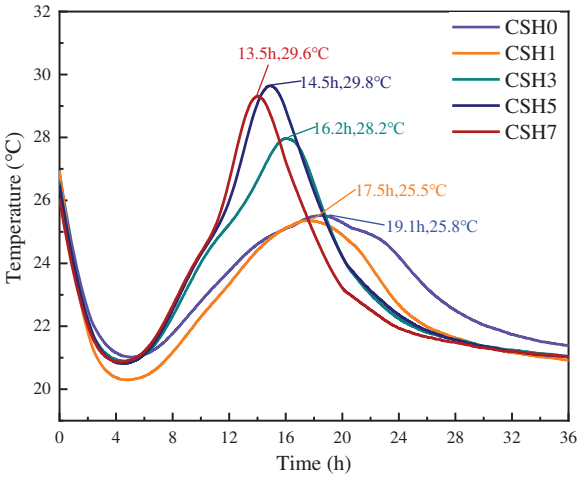

Figure 5: Effects of CSH on the heat of hydration

As the CSH suspension contains a certain amount of superplasticizers, the superplasticizers, when incorporated into the cement paste, can delay its induction period and attenuate the hydration exothermic peak [52]. From Fig. 5, the addition of 1% CSH can compensate partly or completely for this retardation effect. Therefore the peak hydration exothermic strength of the slurry containing 1% CSH is essentially the same as that of the control, but the peak appears earlier. In addition, the hydration temperature of the slurry increases with the accelerated action of the CSH crystal seed. This increase in hydration temperature promotes the development of concrete strength. Concrete with CSH crystal seed exhibits excellent compressive strength in the early stages. The hydration heat flow curve corresponds to the trend in setting time (Fig. 3) and early compressive strength (Fig. 4). The earlier the peak exothermic value appears, the faster the cement paste sets and the early compressive strength is increased.

3.5 FT-IR Analysis

FT-IR was a common research method in materials and was also widely used in cement-based materials [53–57]. FT-IR could sensitively detect the change of Si-O bond in cement paste and had certain advantages in analyzing the change of hydration product C-S-H gel. Fig. 6 shows the FT-IR spectra of paste hydrated for 12 and 24 h with different CSH contents. For the infrared absorption spectrum of cement, the silicon oxide tetrahedron in the main mineral tricalcium silicate and dicalcium silicate exists as an island, Q^0. The expansion vibration of its Si-O would produce an absorption peak near 925 cm^{-1} [55,56]. When reacting with water, the silicon oxide tetrahedron polymerizes into a Si-O-Si bond. Q^0 changed to Q^2, and the vibration absorption peak shifted to a high wave number [54,56]. Cement hydration generated a large amount of C-S-H gel (or tobermorite), and the vibration absorption peak of Q^2 in the silica tetrahedron was around 970 cm^{-1} [56]. In Fig. 6a, with the increase of the content of CSH, the peak waved number corresponding to Q^2 in the sample shifted from 970 to 976 cm^{-1}, which indicated that the silica tetrahedron in C-S-H gel had a high degree of polymerization near 976 cm^{-1}, and the peak intensity and peak area corresponding to Q^2 increase with it.

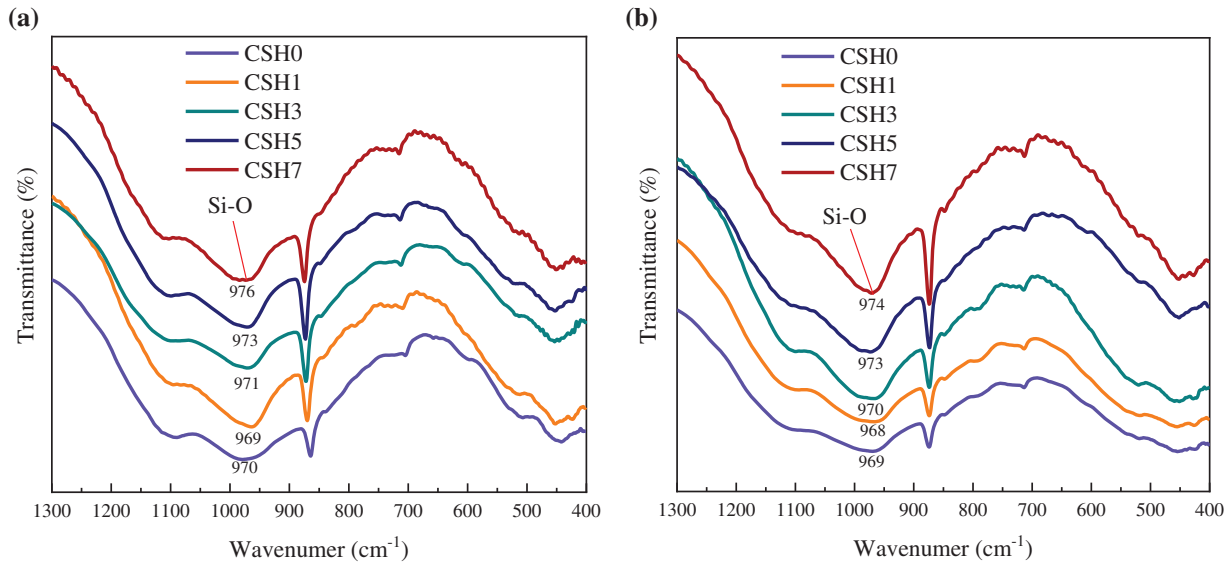

Figure 6: FT-IR spectra of paste with different CSH contents: (a) 12 h, (b) 24 h

The 12 and 24 h FT-IR results were consistent. According to the research [58], if the Si-O bond stretching vibration peak in C-S-H gel moved to a higher wave number and the peak area kept increasing, it indicated that the silica tetrahedron in C-S-H gel had been polymerized to a higher degree. It could be inferred that CSH accelerated the silicate hydration reaction, promoted silica tetrahedron polymerization

in C-S-H gel, and the long chain of silica tetrahedron was easier to form. Which was conducive to the development of early compressive strength of concrete. In addition, some of the C-S-H gel were transformed into tobermorite with high crystallinity, which would be further verified in the subsequent XRD and SEM analyses.

3.6 XRD Analysis

As shown in Fig. 7, the XRD patterns of 12 (a) and 24 h (b) samples with different CSH content were shown. Alizadeh R [35] thought that C-S-H had a structure similar to tobermorite, so there were $2\theta = 32°$ characteristic peaks. The C-S-H (tobermorite) characteristic peak was observed near 32°, and Zhou et al. [36] had similar findings. The existence of silica was also found in the XRD spectrum due to the existence of fly ash, and silica was the main component of fly ash. Compared with the control group, there was no new characteristic peak in the XRD spectrum after the addition of CSH, and the position of the diffraction peak of the corresponding substance had not changed.

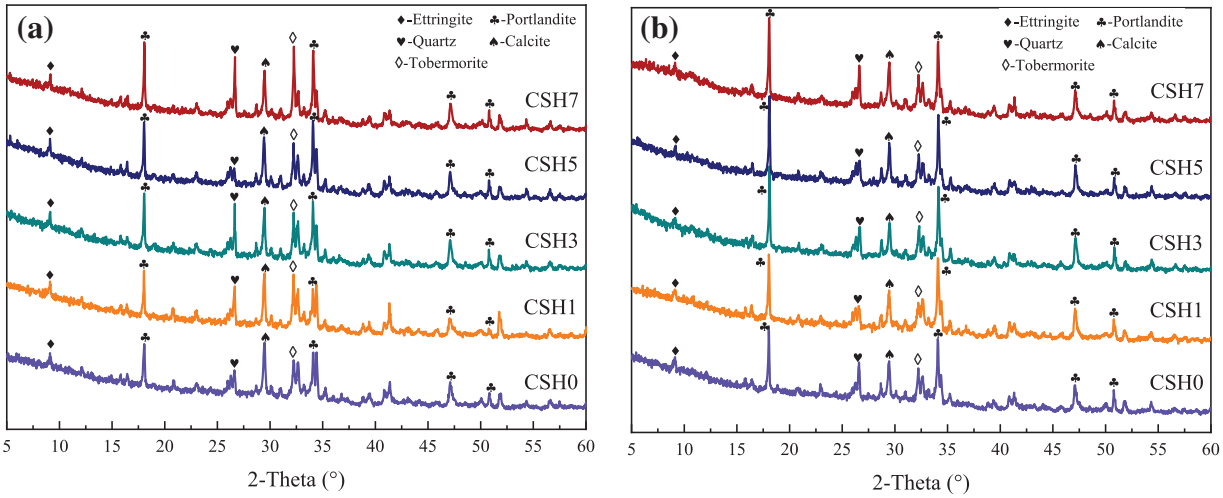

Figure 7: XRD patterns of paste with different CSH contents: (a) 12 h, (b) 24 h

Moreover, the diffraction peak of the hydration products such as C-S-H (tobermorite) and calcium hydroxide in the sample was enhanced, which showed that CSH promoted the hydration of the paste, consistent with the results of hydration temperature analysis and FTIR. C-S-H was the primary source of concrete strength. Concrete would have higher early compressive strength in the presence of CSH, which could be verified from the compressive strength results in Fig. 4.

3.7 SEM Analysis

Fig. 8 shows the morphology comparison of hydration products with different CSH content at 12 (a, b, c) and 24 h (d, e, f) hydration. Fig. 8a shows the morphology of hydration products at 12 h of hydration without CSH. The overall structure of the hydrated product was relatively loose, there were many unhydrated cement particles, and only a tiny amount of C-S-H gel, Ettringite, calcium hydroxide, and other hydrated products were scattered around it. Figs. 8b, 8c were the morphologies of hydrated products of samples hydrated for 12 h with 3% and 7% CSH added, respectively. Compared with Fig. 8a, the number of hydrated products was enhanced, a large number of C-S-H gel filled the pores, and Ettringite and calcium hydroxide were interspersed in the C-S-H gel to form a three-dimensional structure. Figs. 8d, 8e, and 8f show the morphology of the 24 h hydration products corresponding to Figs. 8a, 8b, and 8c, respectively. Different from the hydrated sample hydrated for 12 h, the hydration products shown in Figs. 8d, 8e, 8f are more abundant, and the overall structure was plumper. In addition, the growth state and distribution of

hydration products in the effect of CSH were better than those in the control group. CSH stimulated the paste hydration through the seed effect, which meant that the concrete containing CSH would have more excellent mechanical properties than the control group because the improvement of concrete strength required a large number of hydration products and products to interweave to form a dense three-dimensional structure [37,59].

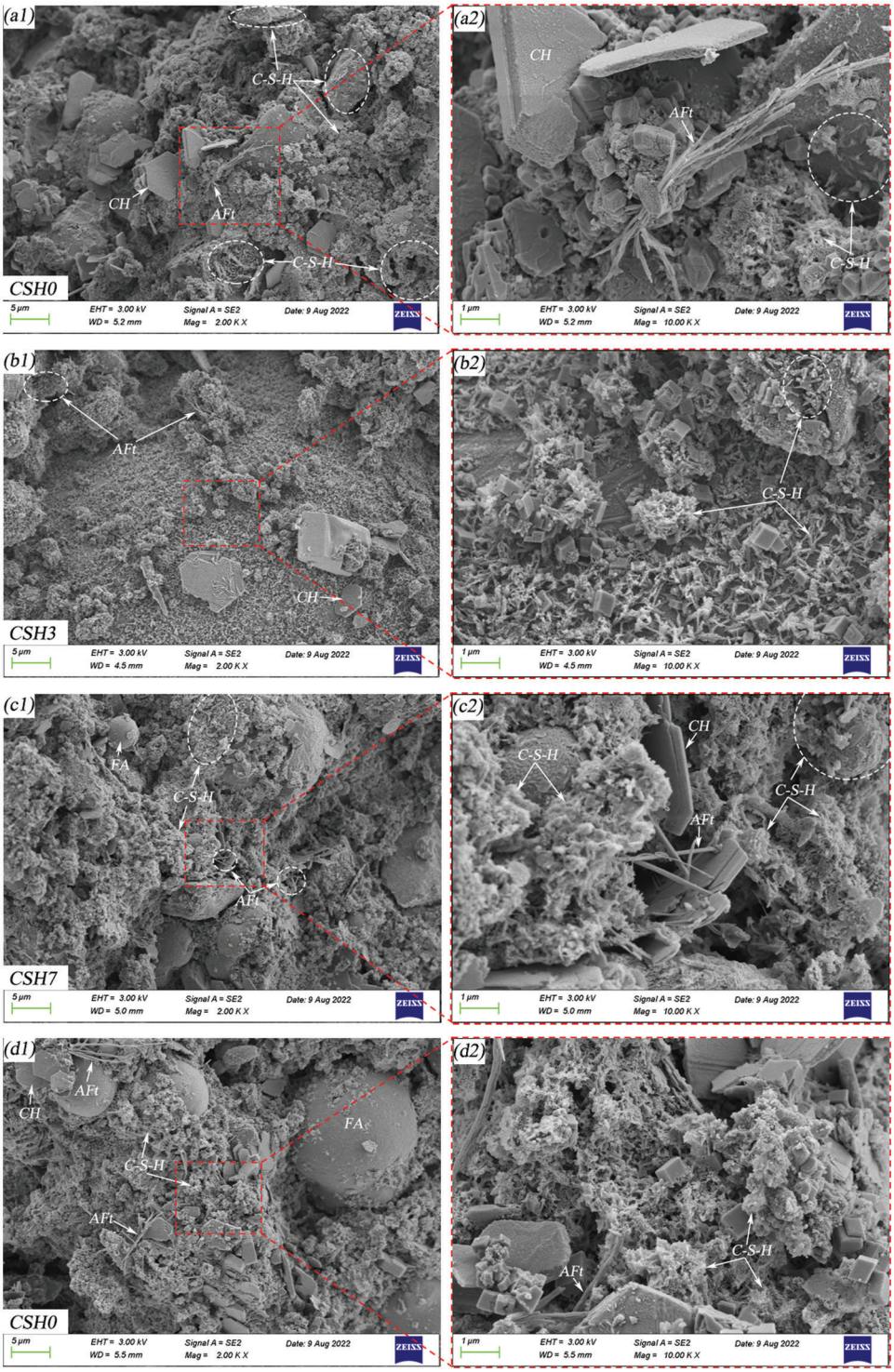

Figure 8: (Continued)

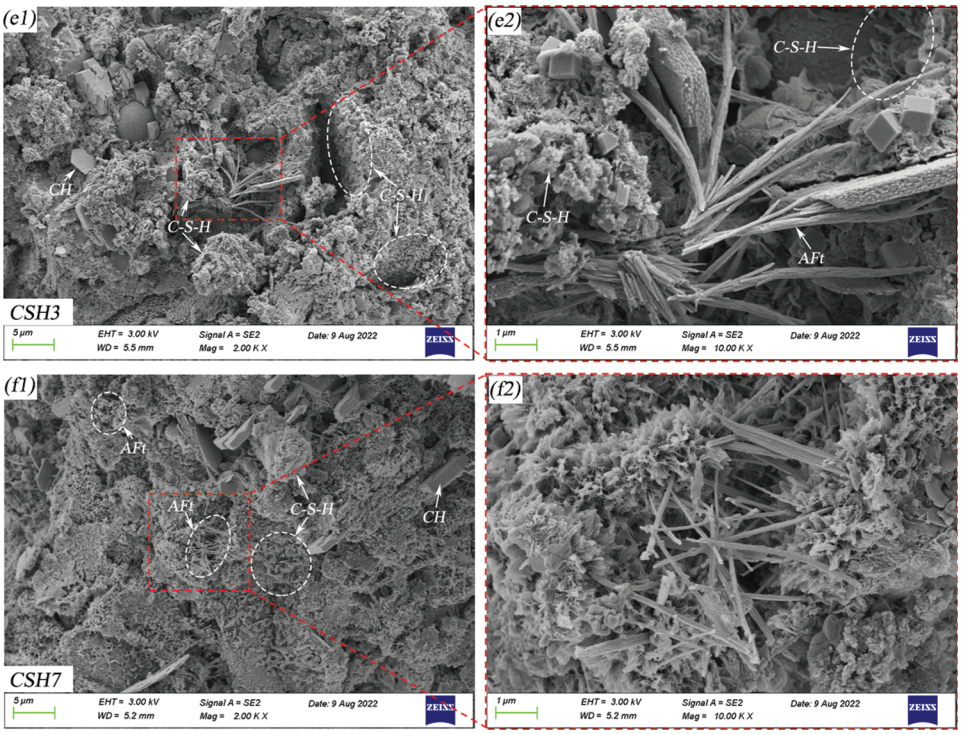

Figure 8: SEM patterns of samples: (a, b, c) hydration products of the cement paste added with 0%, 3% and 7% CSH for 12 h, respectively; (d, e, f) hydration products of the cement paste added with 0%, 3% and 7% CSH for 24 h, respectively

In addition, many materials with uneven edge development and curved sheet shape appeared in the samples containing CSH at 12 or 24 h. As shown in Fig. 9, through energy spectrum analysis and SEM morphology, it could be seen that this crystal phase was tobermorite formed by highly crystallized C-S-H, in which Al^{3+} was also doped, and the existence of Al^{3+} also promoted the formation of tobermorite flake crystal [60]. Which also confirmed the analysis results of XRD and FTIR. Compared with C-S-H gel, tobermorite with good crystallinity could contribute more compressive strength to the matrix, which was also one of the reasons for the excellent strength of CSH concrete.

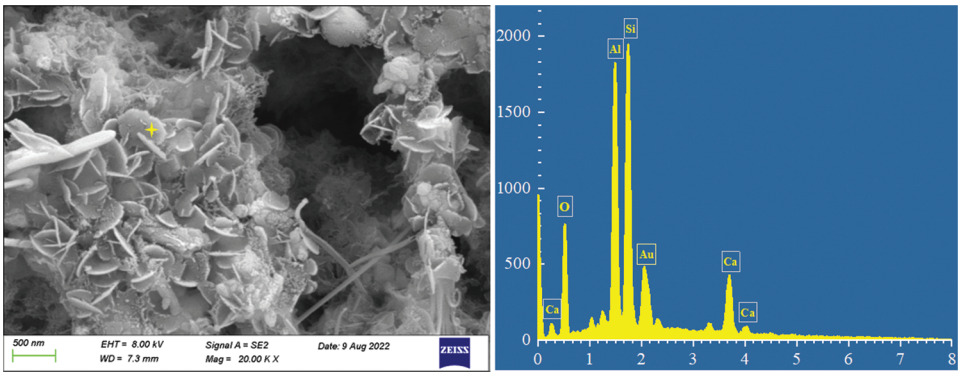

Figure 9: SEM images and the corresponding EDS analysis of typical particle

3.8 Reaction Model

Based on the previous research analysis and related literature [43,48,61–63], a theoretical hydration model of paste containing CSH was given, as shown in Fig. 10. According to relevant literature [63], at the initial stage of cement hydration, the growth of C-S-H gel was preferentially carried out on the surface of cement particles. Because the formation of new nuclei was a process of crystal growth template [64], the surface energy and solubility of the nuclei formed in the cement paste liquid phase in porous solution were very high, so this process required much energy to form a stable growth template [51,62,65]. On the contrary, the nucleation on the cement particle surface had a low surface potential energy for nucleation [48,50]. Therefore, for cement pastes without other CSH seeds, hydration products were formed on the surface of cement particles. However, if there was an established nucleation site in the liquid phase, due to the reduction of the potential nucleation barrier, the hydration products were more likely to have heterogeneous nucleation [37,43,48,50,51,61]. CSH was introduced into concrete as a nucleation seed, which increased the nucleation site and nucleation surface area in the liquid phase, reduced the potential nucleation barrier of hydration products, made C-S-H gel grow preferentially on the surface of CSH seed in the liquid phase [43,61], and also on the surface of cement particles. Which significantly improved the paste hydration speed, manifested in the shortening of the paste setting time, the advance and concentration of the hydration exothermic peak, and the improvement of the early macro mechanical properties. These were also confirmed by the microscopic analysis above.

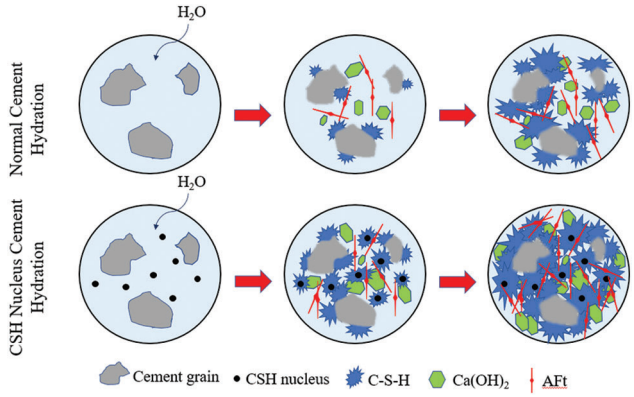

Figure 10: Schematic diagram of hydration with CSH

4 Conclusion

Given the slow development of the early strength of the precast concrete members with a large amount of fly ash, this paper discussed the effect of the new nanomaterial-CSH in concrete. The main conclusions were as follows:

CSH could reduce the dosage of admixture by 47%, significantly shorten the final setting time of the paste, and has no significant impact on the initial setting time, so it would not affect the construction.

CSH significantly improved the early strength of fly ash concrete within 12 h of hydration, with a range of more than 98% at 5% admixture, prompting the mold removal time to be advanced by 12 h.

The CSH shortened the hydration induction period of the paste, made the hydration exothermic peak appear earlier, the exothermic peak was more concentrated, and the peak intensity of the exothermic peak increased. This change was more evident with the increase in the content of CSH.

Through microscopic analysis and reaction modeling, CSH promoted the hydration reaction of cement, using its nucleation effect to lower the reaction's nucleation barrier and promote more hydration products simultaneously.

CSH is one of the cement hydration products and does not introduce other harmful ions. It can be applied to precast components to significantly advance the mold removal time, promote cement hydration, increase strength early, and improve plant production efficiency.

Acknowledgement: The authors would like to thank Zhang Yuyao from Shiyanjia Lab (www.shiyanjia.com) for the XRD analysis.

Funding Statement: The authors received no specific funding for this study.

Conflicts of Interest: The authors declare that they have no conflicts of interest to report regarding the present study.

References

1. Mehta, P. K., Monteiro, P. J. M. (2014). *Concrete: Microstructure, properties, and materials*. New York, Chicago, San Francisco: McGraw-Hill Education.
2. Xi, F., Davis, S. J., Ciais, P. (2016). Substantial global carbon uptake by cement carbonation. *Nature Geoscience, 9(12),* 880–883. https://doi.org/10.1038/NGEO2840
3. Berriel, S. S., Favier, A., Domínguez, E. R. (2016). Assessing the environmental and economic potential of limestone calcined clay cement in cuba. *Journal of cleaner Production, 124,* 361–369. https://doi.org/10.1016/j.jclepro.2016.02.125
4. Environment, U. N., Scrivener, K. L., John, V. M. (2018). Eco-efficient cements: Potential economically viable solutions for a low-CO_2 cement-based materials industry. *Cement and Concrete Research, 114(5),* 2–26. https://doi.org/10.1016/j.cemconres.2018.03.015
5. Golewski, G. L. (2019). The influence of microcrack width on the mechanical parameters in concrete with the addition of fly ash: Consideration of technological and ecological benefits. *Construction and Building Materials, 197(1),* 849–861. https://doi.org/10.1016/j.conbuildmat.2018.08.157
6. Xie, T., Yang, G., Zhao, X. (2020). A unified model for predicting the compressive strength of recycled aggregate concrete containing supplementary cementitious materials. *Journal of Cleaner Production, 251(12),* 119752. https://doi.org/10.1016/j.jclepro.2019.119752
7. Golewski, G. L. (2021). Green concrete based on quaternary binders with significant reduced of CO_2 emissions. *Energies, 14(15),* 4558. https://doi.org/10.3390/en14154558
8. Xu, G., Shi, X. (2018). Characteristics and applications of fly ash as a sustainable construction material: A state-of-the-art review. *Resources, Conservation and Recycling, 136,* 95–109. https://doi.org/10.1016/j.resconrec.2018.04.010
9. Hemalatha, T., Ramaswamy, A. (2017). A review on fly ash characteristics-Towards promoting high volume utilization in developing sustainable concrete. *Journal of cleaner production, 147,* 546–559. https://doi.org/10.1016/j.jclepro.2017.01.114
10. Zhang, D., Ge, Y., Dai, Pang S. (2021). The effect of fly ash content on flexural performance and fiber failure mechanism of lightweight deflection-hardening cementitious composites. *Construction and Building Materials, 302(3),* 124349. https://doi.org/10.1016/j.conbuildmat.2021.124349
11. Szcześniak, A., Zychowicz, J., Stolarski, A. (2020). Influence of fly ash additive on the properties of concrete with slag cement. *Materials, 13(15),* 3265. https://doi.org/10.3390/ma13153265
12. Ahmadi, A., Kianoush, M. R., Moslemi, M. (2021). Investigation on repair of tension cracks in reinforced concrete panels. *Engineering Structures, 245(4),* 112974. https://doi.org/10.1016/j.engstruct.2021.112974

13. Minh, Ha T., Ura, S., Fukada, S. (2020). Development and application of a highly durable precast prestressed concrete slab deck using fly ash concrete. *Structure and Infrastructure Engineering, 16(9),* 1228–1246. https://doi.org/10.1080/15732479.2019.1696377
14. Moffatt, E. G., Thomas, M. D. A., Fahim, A. (2017). Performance of high-volume fly ash concrete in marine environment. *Cement and Concrete Research, 102(11),* 127–135. https://doi.org/10.1016/j.cemconres.2017.09.008
15. Dragaš, J., Ignjatović, I., Tošić, N. (2016). Mechanical and time-dependent properties of high-volume fly ash concrete for structural use. *Magazine of Concrete Research, 68(12),* 632–645. https://doi.org/10.1680/jmacr.15.00384
16. Hemalatha, T., Sasmal, S. (2019). Early-age strength development in fly ash blended cement composites: Investigation through chemical activation. *Magazine of Concrete Research, 71(5),* 260–270. https://doi.org/10.1680/jmacr.17.00336
17. Zou, F., Tan, H., He, X. (2018). Effect of triisopropanolamine on compressive strength and hydration of steaming-cured cement-fly ash paste. *Construction and Building Materials, 192(10),* 836–845. https://doi.org/10.1016/j.conbuildmat.2018.10.087
18. Alghazali, H. H., Aljazaeri, Z. R., Myers, J. J. (2020). Effect of accelerated curing regimes on high volume fly ash mixtures in precast manufacturing plants. *Cement and Concrete Research, 131(12),* 105913. https://doi.org/10.1016/j.cemconres.2019.105913
19. Li, M., Wang, Q., Yang, J. (2017). Influence of steam curing method on the performance of concrete containing a large portion of mineral admixtures. *Advances in Materials Science and Engineering, 2017,* 1–11. https://doi.org/10.1155/2017/9863219
20. Ba, M., Qian, C., Guo, X. (2011). Effects of steam curing on strength and porous structure of concrete with low water/binder ratio. *Construction and Building Materials, 25(1),* 123–128. https://doi.org/10.1016/j.conbuildmat.2010.06.049
21. Liu, B., Shi, J., Zhou, F. (2020). Effects of steam curing regimes on the capillary water absorption of concrete: Prediction using multivariable regression models. *Construction and Building Materials, 256(3),* 119426. https://doi.org/10.1016/j.conbuildmat.2020.119426
22. Xu, Y., He, T., Ma, X. (2022). The influence of calcium nitrate/sodium nitrate on the hydration process of cement paste mixed with alkali free liquid accelerator. *Construction and Building Materials, 347(4),* 128555. https://doi.org/10.1016/j.conbuildmat.2022.128555
23. Ishwarya, G. A., Singh, B., Deshwal, S. (2019). Effect of sodium carbonate/sodium silicate activator on the rheology, geopolymerization and strength of fly ash/slag geopolymer pastes. *Cement and Concrete Composites, 97(202),* 226–238. https://doi.org/10.1016/j.cemconcomp.2018.12.007
24. Zou, F., Tan, H., He, X. (2018). Effect of triisopropanolamine on compressive strength and hydration of steaming-cured cement-fly ash paste. *Construction and Building Materials, 192(10),* 836–845. https://doi.org/10.1016/j.conbuildmat.2018.10.087
25. Xu, Y., He, T. (2021). Effect of nitrate/bromide on the hydration process of cement paste mixed with alkali free liquid accelerator at low temperature. *Crystals, 11(12),* 1585. https://doi.org/10.3390/cryst11121585
26. Yi, Y., Zhu, D., Guo, S. (2020). A review on the deterioration and approaches to enhance the durability of concrete in the marine environment. *Cement and Concrete Composites, 113(4),* 103695. https://doi.org/10.1016/j.cemconcomp.2020.103695
27. Zheng, K., Liu, H., Feng, L. (2021). Effects of calcium-based deicing chemicals on the durability of concrete products. *Journal of Materials in Civil Engineering, 33(11),* 04021321. https://doi.org/10.1061/(ASCE)MT.1943-5533.0003950
28. Nguyen, H. A., Chang, T. P. (2020). Thymotie A. Enhancement of early engineering characteristics of modified slag cement paste with alkali silicate and sulfate. *Construction and Building Materials, 230(7),* 117013. https://doi.org/10.1016/j.conbuildmat.2019.117013
29. Ma, B. G., Xu, X. H. (2006). Effects of triethanolamine on initial structure and mechanical properties of cement. *Journal of Building Materials, 9(1),* 6–9.

30. Sobolev, K., Gutiérrez, M. F. (2005). How nanotechnology can change the concrete world. *American Ceramic Society Bulletin, 84(10),* 14–21.
31. Roychand, R., De Silva S., Setunge, S. (2020). A quantitative study on the effect of nano SiO_2, nano Al_2O_3 and nano $CaCO_3$ on the physicochemical properties of very high volume fly ash cement composite. *European Journal of Environmental and Civil Engineering, 24(6),* 724–739. https://doi.org/10.1080/19648189.2017.1418681
32. Ma, B., Li, H., Li, X. (2016). Influence of nano-TiO_2 on physical and hydration characteristics of fly ash-cement systems. *Construction and building materials, 122,* 242–253. https://doi.org/10.1016/j.conbuildmat.2016.02.087
33. Herath, C., Gunasekara, C., Law, D. W. (2021). Long term mechanical performance of nano-engineered high volume fly ash concrete. *Journal of Building Engineering, 43(8),* 103168. https://doi.org/10.1016/j.jobe.2021.103168
34. Zhang, P., Han, S., Golewski, G. L. (2020). Nanoparticle-reinforced building materials with applications in civil engineering. *Advances in Mechanical Engineering, 12(10),* 1687814020965438. https://doi.org/10.1177/1687814020965438
35. Alizadeh, R., Raki, L., Makar, J. M. (2009). Hydration of tricalcium silicate in the presence of synthetic calcium-silicate–hydrate. *Journal of Materials Chemistry, 19(42),* 7937–7946. https://doi.org/10.1039/b910216g
36. Zhou, Z., Sofi, M., Liu, J. (2021). Nano-CSH modified high volume fly ash concrete: Early-age properties and environmental impact analysis. *Journal of Cleaner Production, 286(3),* 124924. https://doi.org/10.1016/j.jclepro.2020.124924
37. Zhang, C., Cai, Y. (2019). Effects of nano-C-S-H on cement hydration, pore structure of hardened paste and concrete strength. *Journal of the Chinese Ceramic Society, 47,* 585–593. https://doi.org/10.14062/j.issn.0454-5648. 2019.05.01
38. Li, H., Liu, Y., Yang, K. (2022). Effects of synthetic CSH-tartaric acid nanocomposites on the properties of ordinary Portland cement. *Cement and Concrete Composites, 129(3),* 104466. https://doi.org/10.1016/j.cemconcomp.2022.104466
39. Gu, X., Tan, H., He, X. (2022). Nano CSH seed prepared from ground granulated blast-furnace slag-carbide slag and its application in Portland cement. *Construction and Building Materials, 329(2),* 127204. https://doi.org/10.1016/j.conbuildmat.2022.127204
40. Wang, Y., Lu, H., Wang, J. (2020). Effects of highly crystalized nano CSH particles on performances of portland cement paste and its mechanism. *Crystals, 10(9),* 816. https://doi.org/10.3390/cryst10090816
41. Wang, Z., Yao, Y., Tang, R. (2021). The effect and mechanism of C-S–H-PCE nanocomposites on the early strength of mortar under different water-to-cement ratio. *Journal of Building Engineering, 44(2),* 103360. https://doi.org/10.1016/j.jobe.2021.103360
42. Szostak, B., Golewski, G. L. (2021). Rheology of cement pastes with siliceous fly ash and the CSH nano-admixture. *Materials, 14(13),* 3640. https://doi.org/10.3390/ma14133640
43. Wang, F., Kong, X., Jiang, L. (2020). The acceleration mechanism of nano-CSH particles on OPC hydration. *Construction and Building Materials, 249(8),* 118734. https://doi.org/10.1016/j.conbuildmat.2020.118734
44. Land, G., Stephan, D. (2015). Controlling cement hydration with nanoparticles. *Cement and Concrete Composites, 57,* 64–67. https://doi.org/10.1016/j.cemconcomp.2014.12.003
45. Sun, J., Shi, H., Qian, B. (2017). Effects of synthetic CSH/PCE nanocomposites on early cement hydration. *Construction and Building Materials, 140(10),* 282–292. https://doi.org/10.1016/j.conbuildmat.2017.02.075
46. Kanchanason, V., Plank, J. (2017). Role of pH on the structure, composition and morphology of CSH-PCE nanocomposites and their effect on early strength development of Portland cement. *Cement and Concrete Research, 102,* 90–98. https://doi.org/10.1016/j.cemconres.2017.09.002
47. John, E., Matschei, T., Stephan, D. (2018). Nucleation seeding with calcium silicate hydrate–A review. *Cement and Concrete Research, 113,* 74–85. https://doi.org/10.1016/j.cemconres.2018.07.003
48. Thomas, J. J., Jennings, H. M., Chen, J. J. (2009). Influence of nucleation seeding on the hydration mechanisms of tricalcium silicate and cement. *The Journal of Physical Chemistry C, 113(11),* 4327–4334. https://doi.org/10.1021/jp809811w

49. Peng, X. Q., Lan, C. (2015). Influence of hydrated calcium silicate powder on cement hydration reaction process and mechanism. *Journal of Building Materials, 18(2),* 195–201.
50. Nicoleau, L. (2010). New calcium silicate hydrate network. *Transportation Research Record, 2142(1),* 42–51. https://doi.org/10.3141/2142-07
51. Kwon, S. G., Hyeon, T. (2011). Formation mechanisms of uniform nanocrystals via hot-injection and heat-up methods. *Small, 7(19),* 2685–2702. https://doi.org/10.1002/smll.201002022
52. Zhang, Y. R., Kong, X. M., Lu, Z. B. (2015). Effects of the charge characteristics of polycarboxylate superplasticizers on the adsorption and the retardation in cement pastes. *Cement and Concrete Research, 67,* 184–196. https://doi.org/10.1016/j.cemconres.2014.10.004
53. García-Lodeiro, I., Fernández-Jiménez, A., Blanco, M. T. (2008). FTIR study of the sol-gel synthesis of cementitious gels: C-S-H and N-A-S-H. *Journal of Sol-Gel Science and Technology, (45),* 63–72. https://doi.org/10.1007/s10971-007-1643-6
54. Mollah, M. Y. A., Yu, W., Schennach, R. (2000). A Fourier transform infrared spectroscopic investigation of the early hydration of Portland cement and the influence of sodium lignosulfonate. *Cement and Concrete Research, 30(2),* 267–273. https://doi.org/10.1016/S0008-8846(99)00243-4
55. Ghosh, S. N., Handoo, S. K. (1980). Infrared and Raman spectral studies in cement and concrete. *Cement and Concrete Research, 10(6),* 771–782. https://doi.org/10.1016/0008-8846(80)90005-8
56. Sáez del Bosque, I. F., Martínez-Ramírez, S., Blanco-Varela, M. T. (2014). FTIR study of the effect of temperature and nanosilica on the nano structure of C-S-H gel formed by hydrating tricalcium silicate. *Construction and Building Materials, 52,* 314–323. https://doi.org/10.1016/j.conbuildmat.2013.10.056
57. Fernández-Carrasco, L., Torrens-Martín, D., Morales, L. M. (2012). Infrared spectroscopy in the analysis of building and construction materials. *Infrared Spectroscopy-Materials Science, Engineering and Technology, 510*. https://doi.org/10.5772/36186
58. Yu, P., Kirkpatrick, R. J., Poe, B. (1999). Structure of calcium silicate hydrate (C-S-H): Near-, Mid-, and Far-infrared spectroscopy. *Journal of the American Ceramic Society, 82(3),* 742–748. https://doi.org/10.1111/j.1151-2916.1999.tb01826.x
59. Vočka, R., Gallé, C., Dubois, M. (2000). Mercury intrusion porosimetry and hierarchical structure of cement pastes: Theory and experiment. *Cement and Concrete Research, 30,* 521–527. https://doi.org/10.1016/S0008-8846(99)00252-5
60. Tian, H., Stephan, D., Lothenbach, B. (2021). Influence of foreign ions on calcium silicate hydrate under hydrothermal conditions: A review. *Construction and Building Materials, 301,* 124071. https://doi.org/10.1016/j.conbuildmat.2021.124071
61. Ouyang, X., Koleva, D. A., Ye, G. (2017). Insights into the mechanisms of nucleation and growth of C-S-H on fillers. *Materials and Structures, 50(5),* 1–13. https://doi.org/10.1617/s11527-017-1082-y
62. Thanh, N. T. K., Maclean, N., Mahiddine, S. (2014). Mechanisms of nucleation and growth of nanoparticles in solution. *Chemical Reviews, 114(15),* 7610–7630. https://doi.org/10.1021/cr400544s
63. Land, G., Stephan, D. (2012). The influence of nano-silica on the hydration of ordinary Portland cement. *Journal of Materials Science, 47(2),* 1011–1017. https://doi.org/10.1007/s10853-011-5881-1
64. Chu, D. B. K., Owen, J. S., Peters, B. (2017). Nucleation and growth kinetics from LaMer burst data. *The Journal of Physical Chemistry A, 121(40),* 7511–7517. https://doi.org/10.1021/acs.jpca.7b08368
65. Cooper, R. L., Bildsten, L. (2008). Classical nucleation theory of the one-component plasma. *Physical Review E, 77(5),* 056405. https://doi.org/10.1103/PhysRevE.77.056405